PHYSICAL REVIEW B **94**, 220304(R) (2016)

Experimental demonstration of broadband reflectionless diffraction-free electromagnetic wave routing

Youming Zhang,[1] Zhen Gao,[1] Fei Gao,[1] Xihang Shi,[1] Hongyi Xu,[1] Yu Luo,[2] and Baile Zhang[1,3,*]

[1]*Division of Physics and Applied Physics, School of Physical and Mathematical Sciences,Nanyang Technological University, Singapore 637371, Singapore*

[2]*School of Electrical and Electronic Engineering, Nanyang Technological University, Singapore 639798, Singapore*

[3]*Centre for Disruptive Photonic Technologies, Nanyang Technological University, Singapore 637371, Singapore*

(Received 29 March 2016; revised manuscript received 5 December 2016; published 23 December 2016)

Wave diffraction is fundamentally difficult to overcome in the routing and interconnection of photonic signals. Although the phenomenon of reflectionless transport through sharp corners in a routing path has been realized in many previous demonstrations, wave diffraction does not allow them to transport deep-subwavelength information or sub-diffraction-limited images. Recent advances in ε-near-zero and anisotropic ε-near-infinity metamaterials have provided unique possibilities of achieving reflectionless diffraction-free electromagnetic wave routing, but their designs are fundamentally limited to narrow bandwidths, and they have not been demonstrated in reality. Here we experimentally demonstrate broadband reflectionless diffraction-free routing of electromagnetic waves through two right-angled sharp corners in a bent microwave rectangular waveguide. An image with deep-subwavelength information is transported through the bent waveguide in a broad bandwidth. This Rapid Communication supplements and extends the current studies of metamaterials with extreme permittivities and can be useful for routing and interconnection of subwavelength photonic information.

DOI: 10.1103/PhysRevB.94.220304

The wave nature of electromagnetic (EM) radiation imposes a fundamental limitation in the routing and interconnection of photonic signals—the inability of reflectionless diffraction-free transport of EM waves through sharp corners in the propagation path. Previous approaches that can achieve reflectionless transport through sharp corners in the propagation path require complex designs of photonic topological insulators [1–4], which simulate backscattering-immune electronic chiral edge states in topological insulators [5,6] with classical EM waves, or invisibility cloaks [7–9], which hide the corners in an effectively transformed EM space. However, these approaches are still subject to wave diffraction, being unable to deliver deep-subwavelength information or sub-diffraction-limited images.

Recent development in ε-near-zero (ENZ) and anisotropic ε-near-infinity (ENI) metamaterials has provided opportunities to overcome this difficulty. It has been demonstrated that EM waves can tunnel through a narrow waveguide channel filled with ENZ media regardless of the shape of the channel [10–12]. With an additional "sampling" process of inserting stacked thin metallic plates, sub-diffraction-limited images can be delivered through a narrow right-angled bend filled with ENZ media [13]. However, the specific design in the microwave spectrum requires operation at the cutoff frequency of each ultranarrow metallic channel in order to emulate ENZ media [11,13], thus being fundamentally narrow band. Recently, a new type of metamaterial has been proposed, which possesses one permittivity component approaching infinity (we hereafter refer to this type of metamaterial as "single-ENI" media) [14] and can achieve reflectionless diffraction-free wave routing [15] on a two-dimensional (2D) on-chip photonic platform. However, the specific single-ENI design is based on plasmonic resonances among metal/dielectric multilayers, thus being limited to narrow bandwidths as well.

The purpose of this Rapid Communication is twofold. First, we want to demonstrate the reflectionless diffraction-free wave routing phenomenon in reality. Second, we want to achieve a broad working bandwidth. To fulfill this purpose, we propose to utilize double-ENI media (with two permittivity components being infinite at the same time) rather than single-ENI media to demonstrate the broadband reflectionless diffraction-free wave routing phenomenon. The double-ENI media can be realized with a stacking structure of thin metallic plates as inspired by the "sampling" process in Ref. [13]; the detailed construction will be discussed later.

Let us start with the single-ENI media. As shown in Fig. 1(a), a 2D Gaussian beam (waist size of $3\lambda_0$; λ_0 is the free-space wavelength), which is polarized with an in-plane electric field, is incident on the interface between two single-ENI media characterized by the same permittivity tensor of diag$\{\varepsilon_\parallel,\varepsilon_\perp,\varepsilon_\perp\}$ (the subscripts "$\parallel$" and "$\perp$" denote the directions parallel and perpendicular to the optical axis of the medium, respectively), where $\varepsilon_\parallel = \infty$ and $\varepsilon_\perp = \varepsilon_0$ (permittivity of free space). The optical axes (along the direction of $\varepsilon_\parallel$) of the two single-ENI media form angles of 45° with the interface. As predicted in Ref. [15], the Gaussian beam can be bent perfectly with neither reflection nor diffraction. This is because the Gaussian beam propagates as extraordinary waves in both single-ENI media and the extreme anisotropy for extraordinary waves in the single-ENI media fully suppresses wave diffraction. However, when an out-of-plane wave vector is involved, this Gaussian beam will contain not only extraordinary waves, but also ordinary waves, the latter of which are subject to intrinsic diffraction. Even if only extraordinary waves are considered as incident waves, the transmission will be seriously deteriorated [16]. As shown in Fig. 1(b), an incident Gaussian beam of extraordinary

*blzhang@ntu.edu.sg

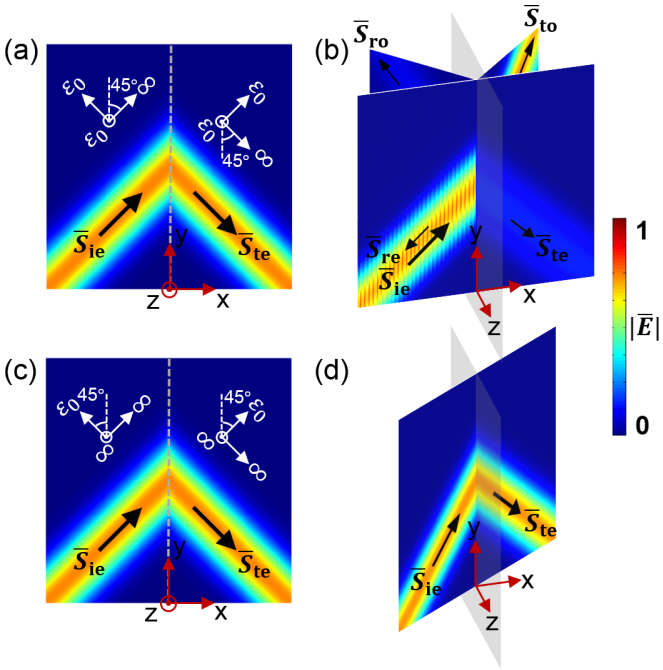

FIG. 1. Wave propagation in single-ENI and double-ENI media. (a) Reflectionless diffraction-free wave bending in single-ENI media in a 2D scenario. (b) Birefringence in single-ENI media when $k_z \neq 0$. (c) Reflectionless diffraction-free wave bending in double-ENI media in a 2D scenario. (d) Reflectionless diffraction-free wave bending in double-ENI media when $k_z \neq 0$. $\bar{S}_{ie}$, $\bar{S}_{te}$, and $\bar{S}_{re}$ are Poynting vectors of incident, transmitted, and reflected extraordinary waves, respectively. $\bar{S}_{to}$ and $\bar{S}_{ro}$ are Poynting vectors of transmitted and reflected ordinary waves, respectively.

waves with a finite out-of-plane wave-vector component k_z [for illustration purposes, $k_z = 0.5\,k_0$ in Fig. 1(b); k_0 is the wave number in free space] will have a significant portion of energy refracting into ordinary waves when entering the other single-ENI medium. Therefore, the reflectionless diffraction-free wave routing in Fig. 1(a) is limited to 2D beam propagation with a zero out-of-plane wave vector.

A finite out-of-plane wave vector is necessary in guiding and confining wave propagation in a quasi-2D geometry as in most on-chip photonic platforms. Being different from single-ENI media, the reflectionless diffraction-free transmission in double-ENI media is robust to the value of the out-of-plane wave vector. Let us consider a 2D Gaussian beam polarized with an in-plane electric field [the same beam as in Fig. 1(a)] that is incident on the interface between two double-ENI media as shown in Fig. 1(c). Each double-ENI medium has two infinite permittivity components ($\varepsilon_\perp = \infty$ and $\varepsilon_\parallel = \varepsilon_0$ in the permittivity tensor of diag $\{\varepsilon_\parallel, \varepsilon_\perp, \varepsilon_\perp\}$) with the optical axis (along the direction of $\varepsilon_\parallel$) forming an angle of 45° with the interface. Being similar to the case of two single-ENI media in the 2D scenario, the Gaussian beam can be bent perfectly by a right angle without reflection and diffraction. Interestingly, when a finite out-of-plane wave-vector component k_z is involved as shown in Fig. 1(d) ($k_z = 0.5\,k_0$ in the illustration), the reflectionless diffraction-free bending of EM waves can still be achieved.

We explain the origin of diffraction-free property and the difference between single-ENI and double-ENI media here. The diffraction-free property of single-ENI media stems from the flat dispersion of the extraordinary waves. Such a flat dispersion supports a real infinite value of the transverse wave vectors and meanwhile guarantees a same phase accumulation while the extraordinary waves propagate [15]. However, in the routing design of single-ENI media, when there is a finite out-of-plane wave vector as requested by the guidance condition of a quasi-2D platform, ordinary waves will be involved when the extraordinary waves go through the boundary, and the birefringent effect will deteriorate the reflectionless diffraction-free transmission. On the other hand, the isofrequency surface of ordinary waves in double-ENI media is a spherical surface with an infinite radius, meaning that ordinary waves are always suppressed in double-ENI media. Thus, the birefringence issue as in single-ENI media will not occur in double-ENI media. Moreover, the isofrequency surface of extraordinary waves in double-ENI media is an infinitely long cylindrical surface oriented along the optical axis. On any plane where the optical axis lies, the dispersion shares the same flatness as in single-ENI media, being able to support real infinite wave vectors and suppress wave diffraction in the direction of the optical axis. Hence, the waves in double-ENI media are undisturbed by a birefringent effect and are free of diffraction in the direction of the optical axis.

We now calculate the general condition of perfect transmission between two double-ENI media in detail. We consider an interface (y-z plane) between two double-ENI media, whose isofrequency surfaces of extraordinary waves are shown in Fig. 2. The optical axes of medium 1 and medium 2 are O_1 and O_2 on the x-y plane, forming angles of θ_1 and θ_2 with the interface, respectively. The finite permittivity components $\varepsilon_\parallel$ of medium 1 and medium 2 are ε_1 and ε_2. An EM wave with an arbitrary extraordinary wave-vector $\bar{\boldsymbol{k}}_{ie} = \hat{\boldsymbol{y}}k_y + \hat{\boldsymbol{z}}k_z + \hat{\boldsymbol{x}}\sqrt{|\bar{\boldsymbol{k}}_{ie}|^2 - k_y^2 - k_z^2}$ (k_y and k_z are arbitrary, satisfying $|\bar{\boldsymbol{k}}_{ie}|^2 - k_y^2 - k_z^2 > 0$) is incident from medium 1 to medium 2. By matching boundary conditions [16], we obtain the general condition of perfect transmission between two double-ENI media as

$$\sqrt{\varepsilon_1 \frac{\omega^2}{c^2} - k_z^2}\,\cos(\theta_2) = \sqrt{\varepsilon_2 \frac{\omega^2}{c^2} - k_z^2}\,\cos(\theta_1), \qquad (1)$$

where c is the light speed in free space. The perfect transmission condition in Eq. (1) involves: (i) the finite permittivity components ε_1 and ε_2 of the two media, (ii) angles θ_1 and θ_2 between each optical axis of the two media and the interface, (iii) the frequency ω, and (iv) the out-of-plane wave-vector component k_z. We consider two cases in the following.

Case 1 $k_z = 0$. In this 2D case, the electric fields are all in plane (i.e., $E_z = 0$). The perfect transmission condition in Eq. (1) becomes $\sqrt{\varepsilon_1}\cos(\theta_2) = \sqrt{\varepsilon_2}\cos(\theta_1)$, which means the reflectionless diffraction-free transmission is irrelevant to either the frequency or the incident angle $\alpha_i = \arcsin(k_y/|\bar{\boldsymbol{k}}_{ie}|)$. This 2D scenario of perfect transmission in double-ENI media is similar to that of single-ENI media [15] and can be applied to route, squeeze, and dilute EM waves.

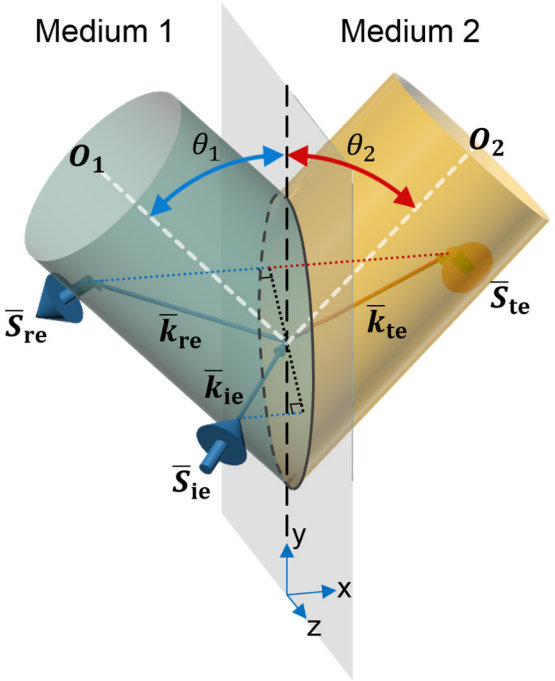

FIG. 2. Isofrequency surfaces of extraordinary waves incident at an interface between two double-ENI media. The optical axes $\boldsymbol{O}_1$ and $\boldsymbol{O}_2$ (white dashed lines) of the two media are on the x-y plane forming angles of θ_1 and θ_2 with the interface ($y-z$ plane). $\bar{\boldsymbol{k}}_{\mathbf{ie}}$, $\bar{\boldsymbol{k}}_{\mathbf{re}}$, and $\bar{\boldsymbol{k}}_{\mathbf{te}}$ ($\bar{\mathbf{S}}_{\mathbf{ie}}$, $\bar{\mathbf{S}}_{\mathbf{re}}$, and $\bar{\mathbf{S}}_{\mathbf{te}}$) are wave (Poynting) vectors of incident, reflected, and transmitted extraordinary waves, respectively.

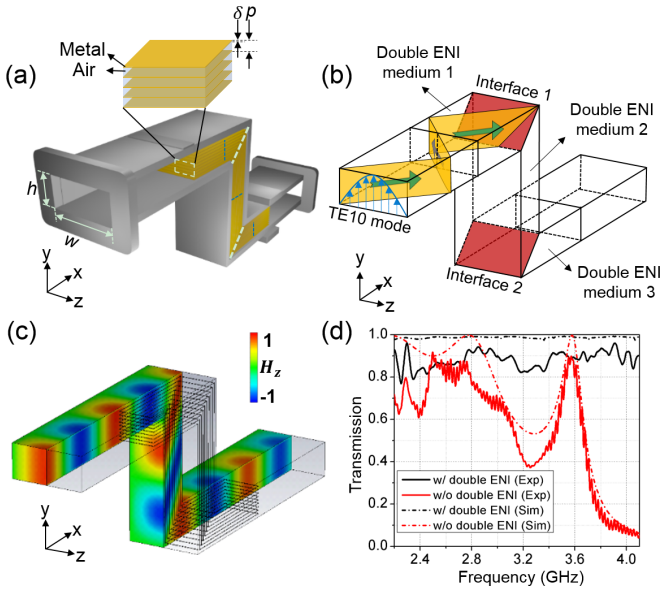

FIG. 3. Verification of reflectionless transmission in double-ENI media. (a) Schematic of the homemade rectangular waveguide with two right-angle sharp corners filled with metallic-plate-stacking metamaterials. The port dimensions of the waveguide are $w = 72$ and $h = 34$ mm. The white dashed lines show two interfaces. The blue dashed lines show the directions of the optical axes. (b) Illustration of the equivalent media distribution and the wave propagation of the TE10 mode in the geometry of the waveguide. (c) Simulated magnetic-field distribution at 3.2 GHz. (d) Measured and simulated transmissions through the bent waveguide with/without double-ENI metamaterial structures.

Case 2 $k_z \neq 0$. The wave propagation in this case is beyond 2D. When and only when $\varepsilon_1 = \varepsilon_2$ and $\theta_1 = \theta_2$ are satisfied in Eq. (1) can the perfect transmission be independent of the frequency, the incident angle $[\alpha_i = \arcsin(\sqrt{k_y^2 + k_z^2}/|\bar{\boldsymbol{k}}_{\mathbf{ie}}|)]$, and the out-of-plane wave-vector component k_z. Otherwise, the perfect transmission occurs only at a single frequency. In the following experimental demonstration, we adopt the conditions of $\varepsilon_1 = \varepsilon_2$ and $\theta_1 = \theta_2$ for a broad working bandwidth.

We now demonstrate the broadband reflectionless diffraction-free wave routing phenomenon of double-ENI media with metallic-plate-stacking metamaterials. A homemade rectangular waveguide with two right-angle sharp corners is illustrated in Fig. 3(a). Thin metallic plates (thickness of $\delta = 0.4$ mm) stacked periodically (period $p = 3.4$ mm) are inserted into the waveguide as double-ENI media. Indeed, this double-ENI design matches the "sampling" region in Ref. [13]. We can understand the value of each effective permittivity component in the following manner. When the electric field is perpendicular to the thin metallic plates, the waves in fact do not "feel" the existence of these metallic plates. This is exactly the reason for the zero reflection in Ref. [13] when the waves of the TE10 mode enter the "sampling" region. Therefore, in the stacking direction, the effective permittivity component ($\varepsilon_{\parallel}$) is just the permittivity of air (ε_0) in the setup. On the other hand, electric fields parallel to the thin metallic plates are required to be zero at the surface of each metallic plate. As the metallic plates are stacked at the deep-subwavelength scale, in the bulk metallic-plate-stacking structure, the average electric field in the two directions parallel to the metallic plates is almost zero. Therefore, the effective permittivity components ($\varepsilon_{\perp}$) in these two directions are both infinite.

An explicit calculation of effective permittivity components from effective medium theory can be conducted as follows. For a multilayer structure consisting of two constituents with permittivity of ε_1 and ε_2 and filling factors of f and $1-f$, the effective permittivity components can be obtained according to the following standard formulas [17,18]:

$$\varepsilon_{\mathrm{eff}\perp} = \varepsilon_1 f + \varepsilon_2(1-f), \tag{2}$$

$$\varepsilon_{\mathrm{eff}\parallel} = \frac{\varepsilon_1\varepsilon_2}{(1-f)\varepsilon_1 + f\varepsilon_2}. \tag{3}$$

It is well known that in the frequency spectrum ranging from microwave to far infrared, metals can be treated as perfect electric conductors that have infinite permittivity [19,20]. Thus in our calculation, $\varepsilon_1 = \infty, \varepsilon_2 = \varepsilon_0$, and $f = \delta/p \ll 1$, which result in $\varepsilon_{\mathrm{eff}\perp} = \infty$ (in two directions) and $\varepsilon_{\mathrm{eff}\parallel} = \varepsilon_0$ (in one direction). The values of these effective permittivity components are further verified with numerical simulations [16]. Similar metamaterial structures have been adopted previously in designs of unconventional lenses with subwavelength resolution [21,22].

The equivalent geometry of the waveguide filled with double-ENI media is illustrated in Fig. 3(b). In the same $x-y-z$ coordinate system, the double-ENI media 1 and 3

have a permittivity tensor of diag $\{\infty, \varepsilon_0, \infty\}$, and the double-ENI medium 2 has a permittivity tensor of diag $\{\varepsilon_0, \infty, \infty\}$. Since the optical axes [blue dashed lines in Fig. 3(a)] of double-ENI media filled in the waveguide form the same angle of 45° with the interface [white dashed lines in Fig. 3(a) or red planes in Fig. 3(b)] between each pair of adjacent double-ENI media, the general perfect transmission condition in Eq. (1) is satisfied. We adopt the fundamental waveguide mode (TE10 mode) for demonstration. Note that the waves of the TE10 mode follow a zigzag path in the waveguide as illustrated in Fig. 3(b), exhibiting a finite out-of-plane wave-vector component k_z. The transverse standing wave along the z direction can be treated as the superposition of two plane waves with opposite k_z values. Because these two plane waves are fully mirror symmetric with respect to the $x - y$ plane, the transmission of the TE10 mode through the waveguide is equivalent to the transmission of a single plane wave with the finite k_z through the corresponding metallic-plate-stacking metamaterial structure that is infinite along the z direction. Therefore, the setup of the bent waveguide can demonstrate the unique advantage of double-ENI media as illustrated in Fig. 1(d). A full-wave simulation for the corresponding metallic-plate-stacking metamaterial structure that is infinite along the z direction is provided in the Supplemental Material [16].

We choose the working frequency range from 2.2 to 4.1 GHz in which only the waves of the TE10 mode can propagate in the waveguide. The magnetic-field distribution at 3.2 GHz simulated with CST MICROWAVE STUDIO is shown in Fig. 3(c). Almost perfect transmission through the bent waveguide can be observed. The measured transmission over the broad frequency range from 2.2 to 4.1 GHz in Fig. 3(d) shows that the waveguide filled with double-ENI media can reach almost unity transmission with only slight transmission reduction compared to the simulation results. The slight transmission reduction is mainly due to the manufacturing imperfection and the coupling loss from the homemade waveguide to the vector network analyzer. In contrast, the empty bent waveguide without double-ENI media shows significantly reduced transmission, whose resonant spectral shape is a result of the structural resonance formed between the two right-angle sharp corners. Note that there is also a slight reduction in transmission through the empty waveguide compared to the simulation results. This further confirms that the slight transmission reduction is from the measurement setup, rather than from the double-ENI media.

Finally, we demonstrate that the double-ENI media can deliver deep-subwavelength information through sharp corners. A metallic mask with two subwavelength slits (width 3.4 mm) separated by a center-center distance of $d = 6.8$ mm as shown in the inset of Fig. 4(a) is attached to the input of the double-ENI metamaterial structure. We illuminate the mask by launching waves from the left port of the waveguide. The field distribution at the output of the double-ENI metamaterial structure is measured with a near-field probe [16]. As the

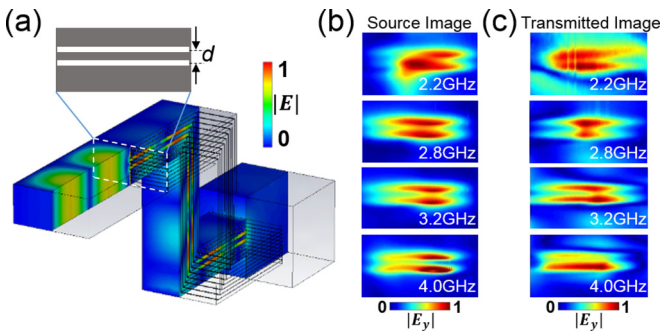

FIG. 4. Demonstration of diffraction-free subwavelength information transmission. (a) Simulated electric-field $|\boldsymbol{E}|$. A metallic mask with subwavelength slits (width of 3.4 mm; center-to-center distance of $d = 6.8$ mm) is attached on the right side of the double-ENI metamaterial structure. The field at the output of the double-ENI metamaterial structure diffracts into free space. (b) Measured source images at different frequencies. (c) Measured transmitted images at different frequencies.

simulated electric-field distribution in Fig. 4(a) shows, the waves emitted from the two subwavelength slits are routed through the bent waveguide. Note that at the output the waves will diffract into free space. This will cause reflection and form standing waves in the two subwavelength wave channels. We plot the measured source image (field distribution immediately behind the mask) in Fig. 4(b) and the measured transmitted image (field distribution immediately behind the double-ENI metamaterial structure) in Fig. 4(c). It is evident that the image with deep-subwavelength information can be transmitted through the bent waveguide with two sharp corners in a broad bandwidth.

The above results demonstrate for the reflectionless diffraction-free wave routing of EM waves over a broad bandwidth. The extension from single-ENI media into double-ENI media for wave routing applications beyond 2D is proposed as inspired by the "sampling" region in the previous ENZ design utilizing a metallic-plate-stacking metamaterial. Particularly, an image with deep subwavelength information transported through two sharp corners in a bent waveguide in a broad bandwidth. As a supplement and extension of the current studies of metamaterials with extreme permittivities, this Rapid Communication may find novel use in high-efficiency deep-subwavelength information routing and interaction in photonic systems.

This work was sponsored by the NTU-NAP Start-Up Grant, Singapore Ministry of Education under Grants No. MOE2015-T2-1-070 and No. MOE2011-T3-1-005. Y.L. would like to acknowledge funding support from the Singapore Ministry of Education under Grant No. MOE2015-T2-1-145, a Singapore NRF-CRP Grant (Grant No. NRF2015NRF-CRP002-008), and the Program Grant (Grant No. 11235150003) from NTU-A*STAR Silicon Technologies Centre of Excellence.

[1] Z. Wang, Y. Chong, J. D. Joannopoulos, and M. Soljacic, Nature (London) **461**, 772 (2009).

[2] W.-J. Chen, S.-J. Jiang, X.-D. Chen, J.-W. Dong, and C. T. Chan, Nat. Commun. **5**, 5782 (2014).

[3] L. Lu, J. D. Joannopoulos, and M. Soljacic, Nat. Photonics **8**, 821 (2014).
[4] X. Cheng, C. Jouvaud, X. Ni, S. H. Mousavi, A. Z. Genack, and A. B. Khanikaev, Nature Mater. **15**, 542 (2016).
[5] M. Z. Hasan and C. L. Kane, Rev. Mod. Phys. **82**, 3045 (2010).
[6] X. L. Qi and S. C. Zhang, Rev. Mod. Phys. **83**, 1057 (2011).
[7] J. B. Pendry, D. Schurig, and D. R. Smith, Science **312**, 1780 (2006).
[8] U. Leonhardt, Science **312**, 1777 (2006).
[9] S. Xu, H. Xu, H. Gao, Y. Jiang, F. Yu, J. D. Joannopoulos, M. Soljačić, H. Chen, H. Sun, and B. Zhang, Proc. Natl. Acad. Sci. USA **112**, 7635 (2015).
[10] M. G. Silveirinha and N. Engheta, Phys. Rev. Lett. **97**, 157403 (2006).
[11] B. Edwards, A. Alù, M. E. Young, M. Silveirinha, and N. Engheta, Phys. Rev. Lett. **100**, 033903 (2008).
[12] R. Liu, Q. Cheng, T. Hand, J. J. Mock, T. J. Cui, S. A. Cummer, and D. R. Smith, Phys. Rev. Lett. **100**, 023903 (2008).
[13] M. G. Silveirinha and N. Engheta, Phys. Rev. Lett. **102**, 103902 (2009).
[14] P. B. Catrysse and S. Fan, Phys. Rev. Lett. **106**, 223902 (2011).
[15] P. B. Catrysse and S. Fan, Adv. Mater. **25**, 194 (2013).
[16] See Supplemental Material at http://link.aps.org/supplemental/10.1103/PhysRevB.94.220304 for detailed calculation of the transmission in single-ENI and double-ENI media, 3D simulation of the reflectionless diffraction-free wave routing, as well as detailed experimental setups.
[17] G. Milton, *The Theory of Composites* (Cambridge University Press, Cambridge, UK, 2002).
[18] X. Yang, J. Yao, J. Rho, X. Yin, and X. Zhang, Nat. Photonics **6**, 450 (2012).
[19] J. D. Jackson, *Classical Electrodynamics* (Wiley, New York, 1999).
[20] J. A. Kong, *Electromagnetic Wave Theory* (EMW, Cambridge, MA, 2008).
[21] S. Xu, Y. Jiang, H. Xu, J. Wang, S. Lin, H. Chen, and B. Zhang, Sci. Rep. **4**, 5212 (2014).
[22] J. Sun, M. I. Shalaev, and N. M. Litchinitser, Nat. Commun. **6**, 7201 (2015).